Conjoint use of Naphthalene Diimide and Fullerene Derivatives to Generate Organic Semiconductors for n–type Organic Thin Film Transistors

Shailesh S. Birajdar[+],[a, f] Samantha Brixi[+],[b] Pedada Srinivasa Rao,[a, f] Rajesh S. Bhosale,[c] Mohammad Al Kobaisi,[d] Akhil Gupta,*[d] Benoît H. Lessard,*[b] Sidhanath V. Bhosale,*[a, f] and Sheshanath V. Bhosale*[e]

In this paper, we described the design, synthesis, and characterization of two novel naphthalene diimide (NDI) core-based targets modified with terminal fullerene (C_{60}) yield – so called **S4** and **S5**, in which NDI bearing 1 and 2 molecules of C_{60}, respectively. The absorption, electrochemical and thin-film transistor characteristics of the newly developed targets were investigated in detail. Both **S4** and **S5** displayed broad absorption in the 450–500 nm region, owing to the effect of conjugation due to fullerene functionalities. The electrochemical measurement suggested that the HOMO and the LUMO energy levels can be altered with the number of C_{60} units. Both **S4** and **S5** were employed as organic semiconductor materials in n-channel transistors. The thin film transistor based on **S4** exhibited superior electron mobility (μe) values ranging from 1.20×10^{-4} to 3.58×10^{-4} $cm^2\,V^{-1}s^{-1}$ with a current on-off ratio varying from 10^2 to 10^3 in comparison with the performance of **S5** based transistor, which exhibited μe ranging from 8.33×10^{-5} to 2.03×10^{-4} $cm^2\,V^{-1}s^{-1}$ depending on channel lengths.

1. Introduction

The fabrication of organic thin-film transistors (OTFTs) has reached to a level where excellent performance is observed on routine basis.[1] The construction of OTFTs is an important tool to determine charge carriers', i.e. holes and electrons, mobilities of semiconductor materials.[2] To accomplish high OTFT device performance, organic semiconductor materials play an important role.[3] Among the vast variety of organic materials, rylene diimide derivatives, such as naphthalene diimide (NDI) and perylene diimide (PDI), have attracted much attention as these derivatives can be utilized as electron acceptors and n-channel semiconductors for emerging research areas, including OTFTs, organic photovoltaic cells, and organic light emitting diodes, to name a few, mainly due to their high thermal stability, excellent acceptor strength, and ease of synthesis.[4] NDI in particular possesses a planar π-conjugated system and is rigorously investigated due to its tunable optical, electrochemical and electronic properties.[5] Introduction of electron withdrawing moieties at the NDI core positions is known to alter its photophysical, electrochemical and electronic properties to a greater extent.[6] Such core-manipulations and expansions enable further tuning of the energy levels, and the lowest unoccupied molecular orbital (LUMO) level in particular.

The core-functionalized NDIs have been employed for OTFT applications.[7] Over the past few years, several reports have been published where a variety of organic, n-type semiconductors based on NDI format have been investigated. Gao *et al.* reported n-type semiconductors for OTFTs based on core-expanded NDIs fused with 2-(1,3-dithiol-2-ylidene)malonitrile moieties with high electron mobilities values up to 1.2 $cm^2\,V^{-1}s^{-1}$.[8] Würthner *et al.* published core-chlorinated NDI, which in turn exhibited high electron mobility up to

[a] S. S. Birajdar,[+] Dr. P. S. Rao, Dr. S. V. Bhosale
Polymers and Functional Materials Division
CSIR-Indian Institute of Chemical Technology
Hyderabad-500007, Telangana (India)
E-mail: bhosale@iict.res.in
[b] S. Brixi,[+] Prof. B. H. Lessard
Department of Chemical and Biological Engineering,
University of Ottawa
161 Louis Pasteur
Ottawa, Ontario (Canada)
E-mail: benoit.lessard@uottawa.ca
[c] Dr. R. S. Bhosale
Department of Chemistry,
Indrashil University
Rajpur, Mesana, 382470, Gujarat (India)
[d] Dr. M. A. Kobaisi, Dr. A. Gupta
School of Science, Faculty of Science
Engineering and Technology
Swinburne University of Technology
Hawthorn, Victoria 3122 (Australia)
E-mail: akhilgupta@swin.edu.au
[e] Prof. S. V. Bhosale
School of Chemical Sciences
Goa University
Taleigao Plateau, Goa 403206 (India)
E-mail: svbhosale@unigoa.ac.in
[f] S. S. Birajdar,[+] Dr. P. S. Rao, Dr. S. V. Bhosale
Academy of Scientific and Innovative Research (AcSIR)
Ghaziabad - 201 002
Uttar Pradesh (India)
[+] These authors contributed equally to this work.

Supporting information for this article is available on the WWW under https://doi.org/10.1002/open.202000230

8.6 $cm^2 V^{-1} s^{-1}$.[9] The OTFTs based on core-expanded NDIs exhibited electron mobilities up to 3.50 $cm^2 V^{-1} s^{-1}$ and were reported by Zu and co-workers.[10] Facchetti *et al.* reported core-substituted NDI-based, highly soluble and printable n-channel polymer with high electron mobilities values ranging ~0.45–0.85 $cm^2 V^{-1} s^{-1}$ under ambient conditions.[11] More recently, core-substituted NDIs were reported as n-type semiconductors that were stable under OTFT device fabrication conditions.[12] However, the synthesis of core-substituted NDIs derivatized with fullerene substituents and its utilization for OTFT applications has not been achieved to date.

In 1995, Fleming *et al.* suggested fullerene as a promising candidate for n-type thin-film transistors.[13] The electronic properties of fullerene-based devices have improved greatly, achieving electron mobilities of the order 1 $cm^2 V^{-1} s^{-1}$.[14] Recently, C_{60} derivatives have gained much attention for their use in OTFTs and OPVs, mainly due to their reasonable electron mobilities and high solubilities in commonly used and thin-film processing organic solvents.[15] Recently, Hu *et al.* reported imide substituted NDI-fullerene as an interlayer between the pentacene active layer and the gate dielectric, which in turn exhibited filed-effect mobility of 1.76 $cm^2 V^{-1} s^{-1}$ and a current on/off ratio of 10^8.[16]

Therefore, introduction of C_{60} at NDI core-positions is anticipated to realize an efficient acceptor-acceptor (A-A) or A-A-A system and to extend π-conjugation, leading to a deep LUMO energy level and to tune optoelectronic and photophysical properties. Thus, in order to get detailed insight into the impact of fullerene on NDI core in terms of photophysical and electrochemical properties, and on the HOMO and the LUMO energy levels, herein we report two new organic semiconductors, namely NDI–C_{60} (coded as **S4**) and C_{60}NDIC_{60} (coded as **S5**), which are designed based on the conjunction of NDI and C_{60} functionalities (Scheme 1).

It is notable to mention that our aim is to design organic semiconductors based on promising structural formats, of which A-A and A-A-A are favorable types, for OTFT applications. This is in order to utilize NDI functionality that allows core substitutions to generate highly conjugated target structures with strong accepting strengths. Such target structures can fulfil most of the challenging structural requirements of efficient OTFTs. It is worth noting that the inclusion of NDI functionality in a given target is advantageous in terms of enhancing the solubility of that particular target together with the control of photo-physical properties. Moreover, targets based on the A-A and A-A-A formats can be synthesized using simple and scalable synthetic protocols which are paramount for Lab-to-Fab translation. In this study, we prepared solution-processed OTFTs fabricated on rigid substrates. The OTFTs based on S4 exhibited good performance, with electron mobilities values ranging 1.20×10^{-4} to 3.58×10^{-4} $cm^2 V^{-1} s^{-1}$ and a current on-off ratio varying 1×10^2 to 1×10^3, whereas **S5** based transistors exhibited μ_e ranging 8.33×10^{-5} to 2.03×10^{-4} $cm^2 V^{-1} s^{-1}$ depending on channel lengths.

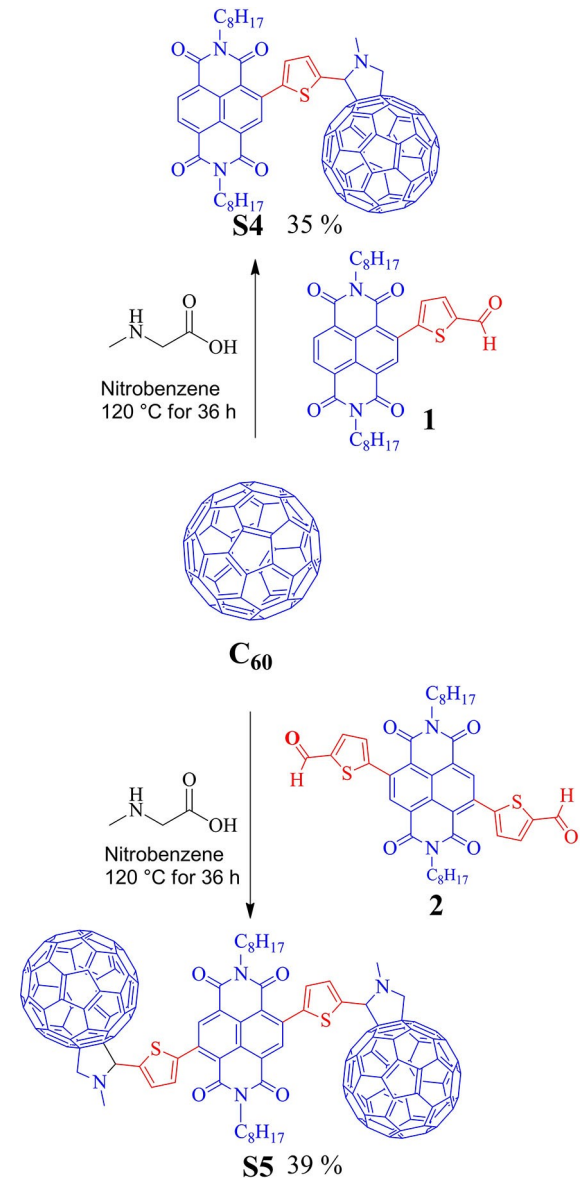

Scheme 1. Synthesis of target **S4** and **S5** dyads.

2. Results and Discussion

2.1. Synthesis and Characterization

The synthetic routes to afford **S4** and **S5** are shown in Scheme 1. The synthesis of intermediates 5-(2,7-dioctyl-1,3,6,8-tetraoxo-1,2,3,6,7,8-hexahydrobenzo[*lmn*][3,8] phenanthrolin-4-yl) thiophene-2-carbaldehyde (**1**) and 5,5′-(2,7-dioctyl-1,3,6,8-tetraoxo-1,2,3,6,7,8-hexahydrobenzo[*lmn*][3,8] phenanthroline-4,9-diyl)bis(thiophene-2-carbaldehyde (**2**) were prepared according to previously reported protocol.[17] Both **S4** and **S5** were synthesized in an identical manner by reacting **1** and **2** intermediates with C_{60} in the presence of sarcosine in nitrobenzene solvent at 120 °C for 36 h, affording **S4** in 35% and **S5** in 39% yields, respectively. The newly synthesized dyad **S4** and triad **S5** were fully characterized by FT-IR, ^{1}H and ^{13}C NMR

spectroscopies, and MALDI-TOF mass characterization techniques, see ESI Figures S1 to S15.

2.2. Thermal Properties

Thermogravimetric analysis (TGA) was run to determine the thermal stabilities of **S4** and **S5 a**re depicted in Figures S16 and S17, respectively. At 5% weight loss, the decomposition temperatures of S4 and S5 are about 398 °C and 395 °C as shown in ESI Figure S16 and S17, respectively. These results clearly indicate that both dyads are thermally stable and can be processed at high temperature to investigate optoelectronic properties.

2.3. Theoretical Calculations

To examine the electronic structures of **S4** and **S5**, theoretical *in vacuo* density functional theory and time dependent-density functional theory (TD-DFT) calculations were performed using the ORCA (Version 4.0.1.2) software package,[18] utilizing Becke's three-parameter Perdew-Wang 1991 (B3PW91) function to consider the non-local, density-dependent dispersion correction (DFT-NL).[18] Because the NL correction significantly enhances the computational cost in particular with the generalized gradient approximations (GGA) treatments using RI, the calculation was conducted in combination with RIJCOSX hybrid functional technique, where the computational overheads are marginal, especially if it is done non-self-consistently. NL method has shown to give the HOMO-LUMO gaps closer to the experimental values, and for fullerene derivatives in particular.[19] The geometric structures of **S4** and **S5** in the ground state were fully optimized at the BP86 level of theory (Figure 1). The DFT calculations indicated that for **S4**, both the HOMO and the LUMO were delocalized over the fullerene moiety, whereas the LUMO + 1 is mainly dispersed on the NDI subunit. For **S5**, the observation of density distribution was almost identical where both the HOMO and the LUMO densities were acquired by the fullerene unit and the LUMO + 1 density was distributed over the NDI unit. The theoretical calculations revealed that for both **S4** and **S5**, the distribution of the HOMO and the LUMO + 1 was well segregated. Thus, the charge separation in the excited state is higher than the ground state. The HOMO energy level of **S4** (−5.74 eV) is lower than **S5** (−5.65 eV), but the LUMO energy levels of **S4** (−4.04 eV) and **S5** (−4.04 eV) are identical. As shown in Figure S18, the density of state (DOS) spectra gave the band gap values of 1.70 eV and 1.61 eV for **S4** and **S5**, respectively, calculated using the Gauss-Sum 3.0 program (see ESI Table S1 and S2).[20] These theoretical results are in good agreement with the experimental data obtained using the absorption and cyclic voltammetry analyses.

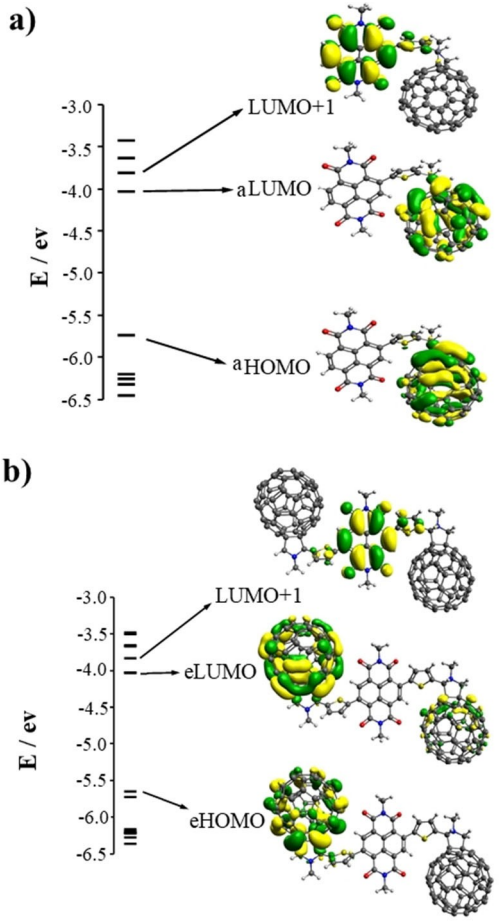

Figure 1. The frontier molecular orbitals (HOMOs, LUMOs, and LUMO + 1 s) and orbital energies of **S4** (**a**) and for **S5** shown in (**b**), by calculated using TD-DFT-NL at the B3PW91/def2-TZVP/J RIJCOSX level of theory.

2.4. Photophysical Properties

The UV-vis absorption spectra of dyad **S4** and triad **S5** in $CHCl_3$ and in pristine thin film are shown in Figures 2a and 2b. In $CHCl_3$, **S4** showed three absorption maxima at 360 nm, 380 nm and 470 nm (broad peak), whereas **S5** exhibited two absorption peaks at 380 nm and a broad intense peak at 490 nm. The absorption peaks appeared in 400–600 nm range correspond to fulleropyrrolidine moieties. In the pristine film form, **S4** displays less intense peaks at 360 nm and 380 nm together with a broad peak at around 490 nm. Pristine film of **S5** exhibited broad absorption maximum at 550 nm with a red-shift of 60 nm, when compared to its solution absorption peak. The absorption onset values of thin film spectra of **S4** and **S5**, i.e. 653 nm and 752 nm, respectively, were utilized to calculate the optical band gap values (**S4** = 1.90 eV and **S5** = 1.65 eV). The bathochromic-shifted absorption maxima of **S4** and **S5** in their thin film forms with respect to their solution spectra are ascribed to the intermolecular π–π stacking interactions between NDI cores.

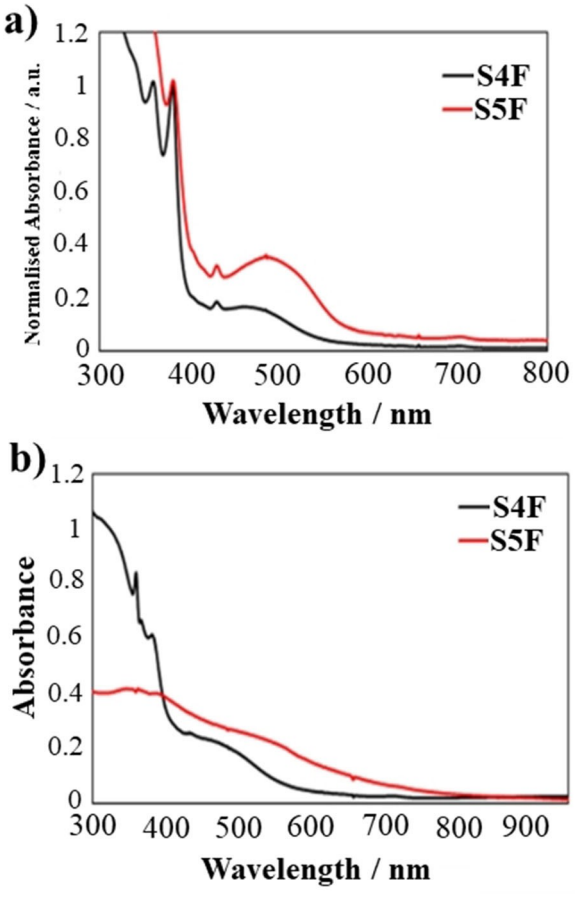

Figure 2. The UV-vis absorption spectra of **S4** and **S5** in $CHCl_3$ solution (**a**), and as a pristine film (**b**).

2.5. Photoelectron Spectroscopy in Air

The photoelectron spectroscopy in air (PESA) measurement was done to estimate the HOMO energy levels (Figure S19) of **S4** and **S5**. The HOMO values of **S4** and **S5** obtained from PESA measurements are −6.01 eV and −5.95 eV, respectively, indicating a good hole blocking ability. By using the HOMO values and the optical band gap (**S4** = 1.90 eV and **S5** = 1.65 eV) values, the calculated LUMO energy levels for S4 and S5 are −4.11 eV and −4.30 eV, respectively. For both S4 and S5, the transition from the HOMO levels to the LUMO energy levels is mainly attributed to S0→S1 transition. The LUMO levels of **S4** and **S5** are comparative to the LUMO level of PCBM (−4.3 eV), suggesting that both the materials, **S4** and **S5** shown to be very good electron mobilities.

2.6. Electrochemical Properties

The electrochemical properties of **S4** and **S5** were investigated using cyclic voltammetry, which was run in dichloromethane and 1,2-dichlorobenzene, respectively, containing 0.1 M of tetra-n-butylammonium hexafluorophosphate. The respective cyclic voltammograms are depicted in Figure 3. The electro-

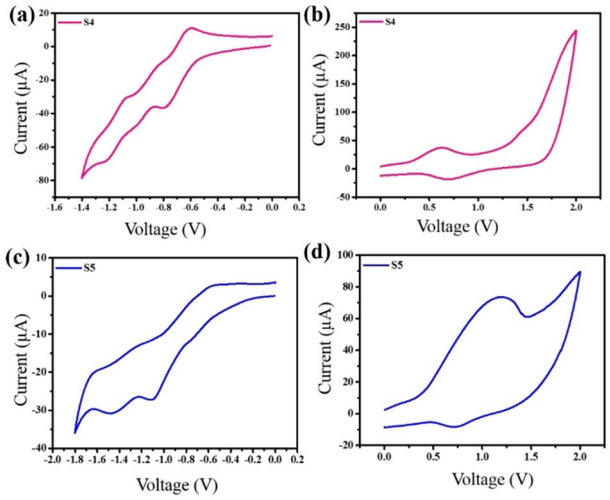

Figure 3. Cyclic voltammograms of **S4** (a & b) and **S5** (c & d) run in dichloromethane and 1,2-diclorobenzene, respectively.

chemical parameters are summarized in Table 1. As shown in Figure 3, both **S4** and **S5** exhibit multiple redox potentials. The first onset oxidation and reduction values are estimated and are displayed in Table 1. These values are utilized to determine the HOMO and the LUMO energy levels of both **S4** and **S5**. The onset oxidation and reduction values of S4 and S5 were estimated to be 0.62 V and 0.72 V, and −0.82 V and −1.1 V, respectively. The calculated HOMO/ LUMO values for **S4** and **S5** were −5.40 eV/−4.00 eV and −5.50/−3.70, respectively. The band gap values of S4 and S5 using cyclic voltammetry were estimated to be 1.40 eV and 1.80 eV, respectively. The HOMO energy level of **S4** is higher when compared with **S5**, a result that suggests superior electron transfer properties of the former.

2.7. OTFT Device Fabrication and Characterization of Semiconducting Properties

Bottom-gate bottom-contact wafers with Si gate OTFT devices were fabricated with the thin films of **S4**, **S5** and $PC_{61}BM$, with the latter as a standard for comparison. The thin-films of **S4** and PCBM were fabricated by spin-coating 10 mg/mL solutions (in chloroform) of respective semiconductors with a spin speed of 1000 rpm. Due to its low solubility in chloroform, the thin films

Table 1. Electrochemical data, the HOMO/LUMO values and the optical band gap values of S4 and S5.

Molecular Structure/ Code	S4	S5
E^{ox}_{onset}(V)	0.62	0.70
E^{red}_{onset}(V)	−0.80	−1.1
HOMO (eV)	−5.40	−5.50
LUMO (eV)	−4.00	−3.70
$E^{el}g$ (ev)[c]	1.40	1.80

$E^{el}g$ (ev): electrochemical band gap determined using cyclic voltammetry.

of **S5** were fabricated by drop-casting a 1 mg/mL solution in *o*-dichlorobenzene. The thin film was dried at 70 °C for 1 h in a vacuum oven to remove residual solvent. The OTFT devices were characterized under vacuum ($P < 0.1$ Pa). The corresponding charge mobility, $I_{on/off}$ ratio and threshold voltages with varying channel lengths were measured.

The device performance results of **S4** are illustrated in Figure 4 and summarized in Table 2. As shown in Figure 4 and Table 2, the thin-film of **S4** shows a n-type semiconductor response with an electron mobility value of 1.20×10^{-4} $cm^2\,V^{-1}\,s^{-1}$ (20 μm channel length), an on/off ratio of 10^2, and a threshold voltage of 22.5 V. As the channel length decreases from 20 μm to 2.5 μm, an increase in the n-type semiconducting properties was observed. As shown in Figure 4 and Table 2, the electron mobility value reaches to 3.58×10^{-4} $cm^2\,V^{-1}\,s^{-1}$, with the on/off ratio of 10^3, and a threshold voltage of 13.4 V, when the 2.5 μm channel length was utilized.

The performance of **S5** is also depicted in Figure 4 and Table 3. At the wider channel length of 20 μm, the electron mobility value is 8.33×10^{-5} $cm^2\,V^{-1}\,s^{-1}$, which enhances to a value of 2.03×10^{-4} $cm^2\,V^{-1}\,s^{-1}$ with the use of a shorter channel length of 2.5 μm. The on/off ratio is 10^2 for 20 μm and 10 μm channel lengths, and 10^3 for 5 μm and 2.5 μm channel lengths, primarily due to a higher mobility at lower channel lengths. Finally, the threshold voltages are 28.0 V and 22.4 V with the use of 20 μm and 2.5 μm channel lengths, respectively.

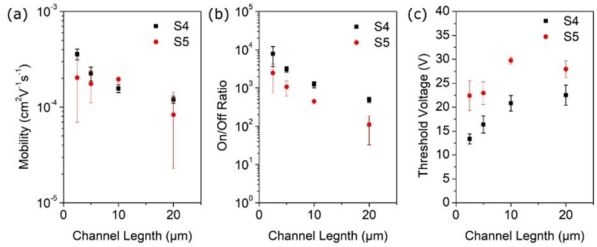

Figure 4. The electron mobility (μ_e) values ($cm^2\,V^{-1}\,s^{-1}$), on/off ratios, and threshold voltages (V_T) for bottom contact OTFT devices based on the pristine films of **S4** and **S5** with varying channel lengths (L) in μm.

Table 2. The OTFT device parameters based on the pristine film of **S4** with varying channel lengths (L). An average of 3 devices is presented at each channel length.

L [μm]	μ_e * [$cm^2\,V^{-1}\,s^{-1}$]	$I_{on/off}$ * (–)	V_T * [V]
20	1.20×10^{-4}	10^2	22.5
10	1.57×10^{-4}	10^3	20.8
5	2.24×10^{-4}	10^3	16.4
2.5	3.58×10^{-4}	10^3	13.4

* μ_e = electron mobility, $I_{on/off}$ = on/off ratio, V_T = threshold voltage.

Table 3. The OTFT device parameters based on the pristine film of **S5** with varying channel lengths (L). An average of 3 devices is presented at each channel length.

L [μm]	μ_e * [$cm^2\,V^{-1}\,s^{-1}$]	$I_{on/off}$ * (–)	V_T * [V]
20	8.33×10^{-5}	10^2	28.0
10	1.95×10^{-4}	10^2	29.7
5	1.75×10^{-4}	10^3	22.9
2.5	2.03×10^{-4}	10^3	22.4

* μ_e = electron mobility, $I_{on/off}$ = on/off ratio, V_T = threshold voltage.

The OTFT performance of **S4** and **S5** was compared with $PC_{61}BM$, given the latter is a benchmark, soluble-processable fullerene derivative (for OTFT results, see Figure S20 and Table S3). The electron mobility values of **S4** and **S5** are lower than the electron mobility of $PC_{61}BM$ ($0.129\,cm^2\,V^{-1}\,s^{-1}$) for 2.5 μm channel length, measured using the bottom-gate bottom-contact method. These results suggest that the addition of a NDI core to the C_{60} system does not enhance electron mobility when compared with the standard $PC_{61}BM$ system.

3. Conclusion

We were able to design, synthetically develop, and characterize two novel organic semiconductors, namely **S4** (a dyad of the type NDI-C60) and **S5** (a triad of the type C60-NDI-C60), which were based on the combination of NDI and C_{60} functionalities. Both **S4** and **S5** were adequately soluble in commonly used, thin-film processing solvents, and exhibited deep LUMO energy levels (~4.0 eV). Given the use of two C_{60} units in **S5**, its absorption was red-shifted when compared with the absorption of its structural analogue **S4**, which utilized one C_{60} unit. The pristine films of **S4** and **S5** were employed in OTFT devices (bottom-gate bottom-contact) where a reasonable performance was observed with the use of a shorter channel length of 2.5 micron. The results of this research evidently suggest that **S4** and **S5** are appropriately designed targets that enrich the library of n-type organic semiconductors for OTFT applications.

Experimental Section

Materials and Methods

All required chemicals were purchased from Sigma-Aldrich and TCI, and the solvents were procured from the commercial suppliers. The NMR spectra (^1H) were recorded at 300 MHz with splitting pattern data noted in part per million (ppm) on the delta scale (δ) and the coupling constants were reported in Hz. The splitting pattern denotes: s (singlet); d (doublet); t (triplet); q (quartet); and m (multiplet). The ^{13}C spectra were recorded at 75 MHz. The IR spectra were recorded on Thermo Nicolet Nexus 670. The mass spectrometry experiments were conducted on Shimadzu Biotech Axima MALDI-TOF MS. The UV-vis spectra were recorded using 1800 Shimadzu spectrophotometer at room temperature (solution concentration = 10^{-5} M). PESA measurements were recorded using a Riken Keiki AC-2 PESA spectrophotometer with a power number of 0.5. Samples for PESA were prepared on ITO cleaned glass substrates and were run using a power setting of 10 nW.

Synthesis of Compound S4

Compound **1** (120 mg, 0.02 mmol) and sarcosine (25 mg, 0.27 mmol) were added to a solution of C_{60} (144 mg, 0.02 mmol) in nitrobenzene (40 mL) at room temperature. The resulting reaction mixture was refluxed for 36 h. The solvent was removed under

reduced pressure. The residue was purified using silica gel column chromatography (eluent: toluene) to yield **S4** (85 mg, yield: 35%) as a brown solid. FT-IR (KBr, cm^{-1}) ν 2921, 2851, 2782, 1705, 1664, 1456, 1434, 1376, 1333, 1309, 1257, 1180, 1029, 787, 769, 526; ^{1}H NMR (300 MHz, $CDCl_3$): δ 0.85–0.88 (m, 6H), 1.27–1.44 (m, 20 H), 1.67–1.75 (m, 4H), 3.02 (s, 3H), 4.07–4.10 (m, 2H), 4.17–4.20 (m, 2H), 4.31–4.32 (d, J = 9.61 Hz, 1H), 5.00–5.02 (d, J = 9.61 Hz, 1H), 5.37 (s, 1H), 7.18–7.19 (d, J = 3.85 Hz, 1H), 7.46–7.47 (d, J = 3.85 Hz, 1H), 8.70 (s, 1H), 8.76 (s, 2H); ^{13}C NMR ($CDCl_3$, 75 MHz): δ 14.42, 22.86, 27.30, 27.59, 28.31, 29.41, 29.52, 29.58, 29.80, 32.04, 40.79, 41.22, 41.49, 68.94, 70.32, 79.53, 124.07, 125.44, 126.57, 126.92, 127.12, 127.96, 130.93, 131.55, 135.84, 136.08, 136.86, 137.22, 140.20, 140.51, 141.81, 142.23, 142.75, 43.16, 143.31, 144.21, 144.54, 144.92, 145.46, 145.73, 146.48, 146.80, 147.30, 153.14, 153.57, 154.03, 155.97, 161.83, 162.58, 162.80; MALDI-TOF: $C_{97}H_{45}N_3O_4S$ *m/z* calculated: 1348.48; found: 1348.86 $[M]^+$ (100%) and 1350.95 $[M+2H]^+$ (80%).

Synthesis of Compound S5

Compound **2** (40 mg, 0.056 mmol) and sarcosine (50 mg, 0.54 mmol) were added to a solution of C_{60} (80 mg, 0.112 mmol) in nitrobenzene (30 mL) at RT. The reaction mixture was heated to 110 °C for 36 h. The solvent was removed under reduced pressure. The residue was purified by column chromatography (silica gel, eluent: toluene) to yield **S5** (45 mg, yield: 39%) as a brown solid. Melting point = 285–287 °C; FT-IR (KBr, cm^{-1}) ν 2919, 2849, 2032, 1703, 1662, 1435, 1376, 1310, 1174, 764, 524; ^{1}H NMR (300 MHz, $CDCl_3$): δ 0.85–0.87 (m, 4H), 1.21–1.27 (m, 20H), 1.53–1.57 (m, 4H), 3.07 (s, 6H), 3.89–3.98 (m, 4H), 4.30–4.32 (d, J = 9.61 Hz, 2H), 5.00–5.02 (d, J = 9.61 Hz, 2H), 5.36 (s, 2H), 7.18–7.19 (d, J = 3.35 Hz, 2H), 7.46–7.47 (d, J = 3.85 Hz, 2H), 8.72 (s, 2H); ^{13}C NMR ($CDCl_3$, 75 MHz): δ 14.39, 23.00, 27.42, 29.64, 30.01, 32.10, 33.54, 40.85, 69.05, 70.43, 79.66, 122.87, 123.54, 125.05, 125.78, 127.12, 128.02, 129.67, 130.65, 135.94, 136.22, 136.45, 136.94, 137.32, 139.14, 139.80, 140.38, 140.46, 140.56, 141.92, 142.41, 142.86, 143.26, 143.37, 144.24, 144.69, 144.95, 145.03, 145.56, 145.83, 146.11, 146.24, 146.38, 146.52, 146.58, 146.65, 147.41,147.64, 148.17, 153.28, 153.69, 154.15, 156.09, 161.98, 162.58; MALDI-TOF: for $C_{164}H_{52}N_4O_4S_2$; *m/z* calculated: 2206.32; found: 2207.42 $[M+H]^+$.

Thermogravimetric Analysis

Thermogravimetric analysis (TGA) experiments were conducted using Q500 TGA instrument with nitrogen as a purging gas. Samples were heated to 800 °C at a heating rate of 10 °C per minute under nitrogen atmosphere.

UV-vis Analysis

The UV-vis absorption spectra were recorded on UV-vis-1800 Shimadzu spectrometer using 1 cm path length quartz cuvette. Aliquots of 300 μL of both **S4** and **S5** (1×10^{-3} M stock solution) were transferred to a glass vial and equilibrate to a final volume of 3 mL (1×10^{-4} M) in dichloromethane. The solutions were allowed to stand for 2 h prior to their spectral measurements. For thin film measurements, samples were prepared onto clean glass substrates using spin coating method.

Cyclic Voltammetry Measurements

The respective solutions of **S4** and **S5** in DCM and 1,2-dichlorobenzene were deoxygenated by bubbling nitrogen gas. Tetra-n-butylammonium hexafluorophosphate (0.1 M) was used as an electrolyte. The cyclic voltammetry experiments were recorded at room temperature by using a PowerLab ML160 potentiostat interfaced *via* a Power Lab 4/20 controller to a PC running E-Chem for Windows version 1.5.2. The cyclic voltammograms were recorded using a standard three electrode configuration with a glassy carbon (2 mm diameter) working electrode, a platinum wire counter electrode and a silver wire pseudo reference electrode. The scans were run with a sweep rate of 50 mV per second. All the potentials were referred to the $E_{1/2}$ of ferrocene/ferrocenium redox couple.

Device Fabrication

Bottom-gate bottom-contact wafers with Si gate, SiO_2 dielectric (t = 230 nm), and Au electrodes (W = 2000 μm, varying L) were purchased from Fraunhofer IPMS. Wafers were washed with acetone, dried, and then treated with plasma for 15 minutes to clean the surface and provide a hydrolyzed surface to be functionalized. The wafers were then submerged in 1% (v/v) octyltricholorosilane in toluene for 1 hour. Following surface treatment, wafers were washed with toluene followed by isopropanol and then dried at 70 °C for 1 hour. The 10 mg/mL solutions of semiconductors in chloroform were spin-coated at 1000 rpm in a glove box and then dried at 70 °C for 1 hour in a vacuum oven to remove residual solvent.

Electrical Characterization

The devices were characterized under vacuum ($P < 0.1$ Pa) using a custom oesProbe A10000-P290 (Element Instrumentation Inc. & Kreus Design Inc.) to enable an inert environment while testing. A Keithley 2614B was used for control of gate-source voltage (V_{GS}) and source-drain voltage (V_{DS}), and to measure source-drain current (I_{DS}). The V_{DS} was set to 50 V for all measurements, while the V_{GS} ranged from 0 to 60 V.

Acknowledgements

S.V.B. (IICT) is grateful for the financial support from the Director, CSIR-IICT, Hyderabad, India (IICT communication number: IICT/Pubs./2020/228). S.S.B. and P.S.R. are grateful for the financial support from the CSIR, New Delhi for SRF fellowship. Authors acknowledge Sharad R. Bobe and Doli Srivani for fruitful discussions. B.H.L acknowledges NSERC DG for the financial support, and S.B. thanks the Ontario government for the Ontario Graduate Scholarship (OGS). S.V.B. (GU) acknowledges UGC-FRP for financial support and Professorship and acknowledges Council of Scientific & Industrial Research (CSIR), India for providing support, code No. 02(0357)/19/EMR-II.

Conflict of Interest

The authors declare no conflict of interest.

Keywords: UV/Vis absorption · electrochemical processes · fullerenes · naphthalene diimide · thin-film transistor

[1] a) M. Krammer, J. W. Borchert, A. Pentritz, E. Karner-Petritz, G. Shider, B. Stadlober, H. Klauk, K. Zojer, *Crystals* **2019**, *9*, 85; b) X. Guo, Y. Xu, S.

Ogier, T. N. Ng, M. Caironi, A. Perinot, L. Li, J. Zhao, W. Tang, R. A. Sporea, et al., *Electron Devices* **2017**, *64*, 1906–1921; c) A. F. Paterson, S. Singh, K. J. Fallon, T. Hodsden, Y. Han, B. C. Schroeder, H. Bronstein, M. Heeney, I. McCulloch, T. D. Anthopoulos, *Adv. Mater.* **2018**, *30*, 1801079.

[2] a) H. Klauk, *Chem. Soc. Rev.* **2010**, *39*, 2643–2666; b) H. Matsui, Y. Takeda, S. Tokito, *Org. Electron.* **2019**, *75*, 105432.

[3] a) A. Facchetti, *Mater. Today*, **2007**, *10*, 28–37; b) J. T. E. Quinn, J. Zhu, X. Li, J. Wang, Y. Li, *J. Mater. Chem. C* **2017**, *5*, 8654–8681.

[4] a) F. Würthener, *Chem. Commun.* **2004**, 1564–1579; b) E. Ahmed, G. Ren, F. S. Kim, E. C. Hollenbeck, S. A. Jenekhe, *Chem. Mater.* **2011**, *23*, 4563–4577; c) X. Wang, J. Huang, Z. Niu, X. Zhang, Y. Sun, C. Zhan, *Tetrahedron* **2014**, ***70***, 4726–4731; d) Y. Liu, L. Zhang, H. Lee, H.-W. Wang, A. Santala, F. Liu, Y. Diao, A. L. Briseno, T. P. Russell, *Adv. Energy Mater.* **2015**, *5*, 1500195; e) D. Srivani, A. Gupta, S. V. Bhosale, K. Ohkubo, R. S. Bhosale, S. Fukuzumi, A. Bilic, L. A. Jones, S. V. Bhosale, *Asian J. Org. Chem.* **2018**, *7*, 220–226; f) M. Korzec, S. Kotowicz, K. Łaba, M. Łapkowski, J. G. Malecki, K. Smolarek, S. Maćkowski, E. Schab-Balcerzak, *Eur. J. Org. Chem.* **2018**, 1756–1760; g) H. F. Higginbotham, P. Pander, R. Rybakiewicz, M. K. Etherington, S. Maniam, M. Zagorska, A. Pron, A. P. Monkman, P. Data, *J. Mater. Chem. C* 2018, 6, 8219–8225; h) T. Weil, T. Vosch, J. Hofkens, K. Peneva, K. Müllen, *Angew. Chem. Int. Ed.* **2010**, *49*, 9068–9093; *Angew. Chem.* **2010**, *122*, 9252–9278; i) A.-J. Payne, N. A. Rice, S. M. McAfee, S. Li, P. Josse, C. Cabanetos, C. Risko, B. H. Lessard, G. C. Welch, *ACS Appl. Energy Mater.* **2018**, *1*, 4906–4916; j) M. Vespa, J. R. Cann, S. V. Dayneko, O. A. Melville, A. D. Hendsbee, Y. Zou, B. H. Lessard, G. C. Welch, *Eur. J. Org. Chem.* **2018**, *33*, 4592–4599; k) A. Laventure, S. Stanzel, A.-J. Payne, B. H. Lessard, G. C. Welch, *Synth. Met.* **2019**, *250*, 55–62.

[5] a) S.-L. Suraru, F. Würthner, *Synthesis* **2009**, *11*, 1841–1845; b) M. Al Kobaisi, S. V. Bhosale, K. Latham, A. M. Raynor, S. V. Bhosale, *Chem. Rev.* **2016**, *116*, 11685–11796.

[6] a) S. Chopin, F. Chaignon, E. Blart, F. Odobel, *J. Mater. Chem.* **2007**,***17***, 4139–4146; b) S. V. Bhosale, C. H. Jani, S. J. Langford, *Chem. Soc. Rev.* **2008**, ***37***, 331–342; c) N. Sakai, J. Mareda, N. Sakai, S. Matile, *Chem. Soc. Rev.* **2010**, *46*, 4225–4237; d) J. Shukla, P. Mukhopadhyay, *Eur. J. Org. Chem.* **2019**, *48*, 7770–7776.

[7] a) L. Polander, S. P. Tiwari, B. M. Seifried, Q. Zhang, S. barrow, C. Risko, J.-L. Brédas, B. Kippelen, S. R. Marder, *Chem. Mater.* **2011**, *23*, 15, 3408–410; b) Y. Zhao, C. Di, X. Gao, Y. Hu, L. Zhang, Y. Liu, J. Wang, W. Hu, D. Zhu, *Adv. Mater.* **2011**, *23*, 268–284; c) D. Hwang, R. Dasari, M. Fenoll, V. Alain-Rizzo, A. Dindar, J. Shim, N. Deb, C. Fuentes-Hernandez, S. Barlow, D. Bucknall, P. Audebert, S. Marder, B. Kippelen, *Adv. Mater.* 2012, ***24***, 4445–4450; d) X. Chen, Y. Guo, L. Tan, G. Yang, Y. Li, G. Zhang, Z. Liu, W. Xu, D. Zhang, *J. Mater. Chem. C* **2013**, *1*, 1087–1092.

[8] a) X. Gao, C. Di, Y. Hu, X. Yang, H. Fan, F. Zhang, Y. Liu, H. Li, D. Zhu, *J. Am. Chem. Soc.* **2010**, *132*, 3697–399; b) Y. Zhao, C. Di, X. Gao, Y. Hu, L. Zhang, Y. Liu, J. Wan, W. Hu, D. Zhu, *Adv. Mater.* **2011**, *23*, 2448–2453; c) Y. Hu, X. Gao, C. Di, X. Yang, F. Zhang, Y. Liu, H. Li, D. Zhu, *Chem. Mater.* **2011**, *23*, 1204–1215.

[9] T. He, M. Solte, F. Würthner, *Adv. Mater.* **2013**, *25*, 6951–6955.

[10] F. Zhang, Y. Hu, T. Schuettfort, C. D. X. Gao, C. R. McNeill, L. Thomsen, S. C. B. Mannsfeld, W. Yuan, H. Sirringhaus, D. Zhu, *J. Am. Chem. Soc.* **2013**, *135*, 2338–2349.

[11] H. Yan, Z. Chen, Y. Zheng, C. Newman, J. Quinn, F. Dotz, M. Kastler, A. Facchetti, *Nature* **2009**, *457*, 679–686.

[12] a) D. Shukla, S. F. nelson, D. C. Freeman, M. Rajeswaran, W. G. Ahearn, D. M. Meyer, J. T. Carey, *Chem. Mater.* **2008**, 20, 7486–7491; b) Y. H. Ha, J. G. Oh, S. Park, S.-K. Kwon, T. K. An, J. Jang, Y.-H. Kim, *Org. Electron.* **2018**, *63*, 250–256; c) H. Ran, L. Chen, X. Y. Jiali, Z. Zhen, Z. Ruijun, H. Xuewei, D. J.-Y. Hu, *Dyes Pigm.* **2019**, *169*, 7–14; d) Q. Ye, J. Chang, K.-W. Huang, X. Shi, J. Wu, C. Chi, *Org. Lett.* **2013**, *15*, 1194–1197; e) J. Xie, K. Shi, K. Cai, D. Zhang, J.-Y. Wang, J. Pei, D. Zhao, *Chem. Sci.* **2016**, 7, 499–504; f) B.-L. Hu, K. Zhang, C. An, W. Pisula, M. Baumgarten, *Org. Lett.* **2017**, *19*, 6300–6303; g) J. Wen, C. Xiao, A. Lv, H. Hayashi, L. Zhang, *Chem. Commun.* **2018**, *54*, 5542–5545.

[13] R. Haddon, A. Perel, R. Morris, T. Palstra, A. Hebard, R. Fleming, *Appl. Phys. Lett.* **1995**, *67*, 121–123.

[14] a) T. D. Anthopoulos, B. Singh, N. Marjanovic, N. S. Sariciftci, A. M. Ramil, H. Sitter, M. Colle, D. M. de Leeuw, *Appl. Phys. Lett.* **2006**, *89*, 213504; b) X. H. Zhang, B. Kippelen, *J. Appl. Phys.* **2008**, 104, 104504; c) X. H. Zhnag, B. Kippelen, *Appl. Phys. Lett.* **2008**, *93*, 133305; d) M. S. Dresselhaus, *Annu. Rev. Mater. Sci.* **1995**, *25*, 487–523.

[15] a) C.-F. Sung, D. Kekuda, L. F. Chu, Y.-Z. Lee, F.-C. Chen, M.-C. Wu, C.-W. Chu, *Adv. Mater.* **2009**, *21*, 4845–4849; b) M. Kitamura, S. Aomori, J. H. Na, Y. Arakawa, *Appl. Phys. Lett.* **2008**, *93*, 033313; c) Y. Zhang, l. Murtaza, H. Meng, *J. Mater. Chem. C* **2018**, *6*, 3514–3537.

[16] J. Tan, J. Sorensen, H. Dong, W. Hu, *J. Mater. Chem. C* **2018**, *6*, 6052–6057.

[17] D. B. Shaikh, A. A. Said, R. S. Bhosale, W. Chen, S. V. Bhosale, A. L. Puyad, S. V. Bhosale, Q. Zhang, *Asian J. Org. Chem.* **2018**, *7*, 2294–2301.

[18] C. Lee, W. Yang, R. G. Parr, *Phys. Rev. B, Condensed matter.* **1988**, 37, 785–789.

[19] H. Wang, Y. He, Y. Li, H. Su, *J. Phys. Chem. A* **2012**. *116*, 255–262.

[20] N. M. O'boyle, A. L. Tenderholt, K. M. Langner, *J. Comput. Chem.* **2008**. *29*, 839–845.

Manuscript received: August 17, 2020
Revised manuscript received: January 9, 2021